Inorganic Chemistry

Article

pubs.acs.org/IC

Four Hybrid Materials Based on Preyssler P_5W_{30} Polyoxometalate and First-Row Transition-Metal Complex

Tuo-Ping Hu,[†,‡] Ya-Qin Zhao,[†] Zvonko Jagličić,[§] Kai Yu,[∥] Xing-Po Wang,[†] and Di Sun*[,†]

[†]Key Lab of Colloid and Interface Chemistry, Ministry of Education, School of Chemistry and Chemical Engineering, Shandong University, Jinan, 250100, P. R. China

[‡]Department of Chemistry, North University of China, Taiyuan, 030051, P. R. China

[§]Faculty of Civil and Geodetic Engineering & Institute of Mathematics, Physics and Mechanics, University of Ljubljana, Jamova 2, 1000 Ljubljana, Slovenia

[∥]School of Chemistry and Chemical Engineering, Harbin Normal University, Harbin 150025, P. R. China

Supporting Information

ABSTRACT: Four Preyssler P_5W_{30} based inorganic−organic hybrids, formulated as $\{[Cu_{12}(pbtz)_2(Hpbtz)_2(OH)_4(H_2O)_{16}][Na(H_2O)P_5W_{30}O_{110}]\}\cdot 16H_2O$ (**1**; H_2pbtz = 5′-(pyridin-2-yl)-1*H*,2′*H*-3,3′-bi(1,2,4-triazole)), $\{[Cu_{10}(ttbz)_2(Httbz)_4(OH)_6(H_2O)_8][K(H_2O)H_2P_5W_{30}O_{110}]\}\cdot 30H_2O$ (**2**; Httbz = 1-(tetrazo-5-yl)-4-(triazo-1-yl)benzene), $\{[Ni_6(bpz)_6(H_2O)_{16}][Na(H_2O)\text{-}H_2P_5W_{30}O_{110}]\}\cdot 36H_2O$ (**3**; bpz = 3,3′,5,5′-tetramethyl-4,4-bipyrazole), $\{[Co_4(bpz)_6(H_2O)_9][K\text{-}(H_2O)H_6P_5W_{30}O_{110}]\}\cdot 46H_2O$ (**4**), have been isolated and structurally identified via microanalysis, thermogravimetry (TG), infrared (IR) spectroscopy, and X-ray single-crystal diffraction. Compound **1** exhibits a 3D binodal (3,6)-connected **ant** framework composed of dodeca-supported P_5W_{30} polyoxometalate (POM) clusters and discrete $[Cu_6(pbtz)(Hpbtz)(OH)_2(H_2O)_8]$ subunits. Compound **2** is a pillared-layer 3D network constructed from $[Cu_5(ttbz)(Httbz)_2(OH)_3(H_2O)_4]$ sheets pillared by individual P_5W_{30} clusters. Compound **3** contains octa-supporting P_5W_{30} POM clusters and novel $[Ni_6(bpz)_6]$ crown-like metallamacrocycles, which construct a (4,4)-connected **pts** network. Compound **4** displays a complicated 3D (5,5)-connected $\{4^5\cdot6^4\cdot8\}\{4^5\cdot6^5\}$ network built by pentasupporting P_5W_{30} POM clusters and discrete $[Co_4(bpz)_6(H_2O)_9]$ subunits. In **1**−**4**, the unified features are the Preyssler-type $[P_5W_{30}O_{110}]$ POM as the fundamental building block, which supports the transition-metal compounds with different modes to give the resultant diverse networks. The magnetism studies indicated antiferromagnetically coupled systems for the hexa- and pentanuclear Cu(II) units in **1** and **2**, respectively. The electrochemical properties demonstrate that all compounds have electrocatalytic abilities toward the reduction of hydrogen peroxide. Furthermore, the catalytic activities of **1** in the cyanosilylation of aldehydes reaction have been investigated.

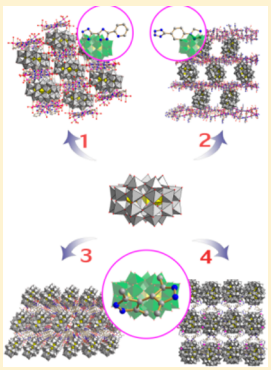

INTRODUCTION

Polyoxometalates (POMs) as an excellent family of inorganic clusters have been attracting widespread attention as they have abundant terminal and bridging O atoms as multidentate O-donor ligands and show tunable acid/base, redox, catalytic, magnetic, and photochemical properties.[1−3] The class of POMs has been known for almost two centuries since the famous Keggin ion $[\alpha\text{-}PMo_{12}O_{40}]^{3-}$ was obtained by Berzelius.[4] In this area, transition-metal coordination complexes (TMCs) are generally employed to decorate classical POMs, such as Keggin-, Lindquist-, Wells−Dawson-, and Anderson-type.[5] Among the documented larger POMs clusters, the Preyssler $[Na(H_2O)P_5W_{30}O_{110}]^{14-}$ anionic cluster possesses doughnut geometry and has recently exhibited distinguished properties in catalysis and magnets.[6] It has rich oxygen donors on the surface for coordination with metal ions and an internal cavity which can encapsulate one alkali or lanthanoid ion;[7] that is to say, this POM could be modified not only on the surface but also in its cavity. In the exterior, including the transition-metal ions, another crucial synthon in building POM based hybrids with versatile topologies rests on the organic ligands, which could impact the coordination modes, conformations, and orientations of metal centers and POM, resulting in novel POM based inorganic−organic hybrids. In the interior, the pristine alkali ion could be replaced by lanthanoid ion to form lanthanoid POMs which have shown possible application in magnetic coolers, quantum computing, and single-molecule magnets.[8] In spite of such a versatile inorganic building block, limited compounds with Preyssler P_5W_{30} as inorganic building block for the construction of modified or extended structures have been reported so far.[9] To our knowledge, the first Preyssler P_5W_{30}-extended network was successfully isolated by Wang et al.[10] Following that, Zhang[11] and Yang[12] groups separately reported some Ln-modified P_5W_{30} based inorganic−organic hybrids and related properties. The main difficulties to access them are the following: (i) growth of a single-crystal with high enough quality for X-ray diffraction, and (ii) exploration of suitable pH

Received: April 29, 2015
Published: July 21, 2015

DOI: 10.1021/acs.inorgchem.5b00962
Inorg. Chem. 2015, 54, 7415−7423

value for self-assembly. These situations motivate us to do such attractive but challenging studies in our lab.[13]

Herein, we systematically explored the reactions of cobalt(II), copper(II), or nickel(II) ions with the Preyssler anions in the presence of different multidentate N-donor ligands (Scheme 1) and have successfully obtained four Preyssler

Scheme 1. Structures of H_2pbtz, Httbz, and bpz Ligands Used in This Work

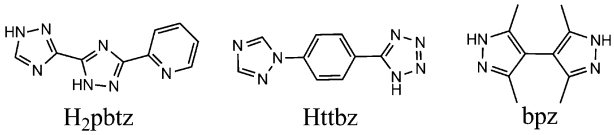

P_5W_{30} based inorganic−organic hybrids, formulated as $\{[Cu_{12}(pbtz)_2(Hpbtz)_2(OH)_4(H_2O)_{16}][Na(H_2O)\text{-}P_5W_{30}O_{110}]\}\cdot 16H_2O$ (**1**; H_2pbtz = 5′-(pyridin-2-yl)-1*H*,2′*H*-3,3′-bi(1,2,4-triazole)), $\{[Cu_{10}(ttbz)_2(Httbz)_4(OH)_6(H_2O)_8][K(H_2O)H_2P_5W_{30}O_{110}]\}\cdot 30H_2O$ (**2**; Httbz = 1-(tetrazo-5-yl)-4-(triazo-1-yl)benzene), $\{[Ni_6(bpz)_6(H_2O)_{16}][Na(H_2O)\text{-}H_2P_5W_{30}O_{110}]\}\cdot 36H_2O$ (**3**; bpz = 3,3′,5,5′-tetramethyl-4,4-bipyrazole), and $\{[Co_4(bpz)_6(H_2O)_9][K(H_2O)\text{-}H_6P_5W_{30}O_{110}]\}\cdot 46H_2O$ (**4**). The common features for them are that they all consist of Preyssler-type $[P_5W_{30}O_{110}]$ POM as the fundamental building block, which supports the transition-metal compounds with different modes to give the resultant diverse networks. The electrochemical behaviors demonstrate that all compounds have electrocatalytic abilities toward the reduction of hydrogen peroxide. The magnetic susceptibility measurements indicate antiferromagnetic coupling interactions within hexa- and pentanuclear Cu(II) units in **1** and **2**. Furthermore, the catalytic activities of **1** in the cyanosilylation of aldehydes have been tested.

EXPERIMENTAL SECTION

Materials and General Methods. $K_{12.5}Na_{1.5}[NaP_5W_{30}O_{110}]\cdot 15H_2O$ was prepared and purified on the basis of known literature methods.[14] The chemical reagents and solvents used in this work were commercially available and used as they are. IR spectra were measured on a Nicolet AVATAT FT-IR360 spectrometer as KBr pellets in the frequency range 400−4000 cm^{-1}. The C, H, N elemental analyses were determined on a Vario EL III analyzer, whereas the K, Na, P, W, and Co analyses were performed by a Leaman inductively coupled plasma (ICP) spectrometer. All ^{1}H NMR spectra were recorded on Bruker-300 MHz spectrometer. Powder X-ray diffraction (PXRD) data were measured on a Philips X'Pert Pro MPD X-ray diffractometer (Cu Kα = 1.5418 Å) with an X'Celerator detector. Thermogravimetric analyses (TGA) were performed on a Netzsch STA 449C thermal analyzer from 30 to 800 °C under nitrogen atmosphere with a heating rate of 10 °C/min. Electrochemical tests were conducted on a electrochemical workstation with model number CHI660. A conventional three-electrode method was used. The working electrode was a carbon paste electrode (CPE), a Pt wire was the counter electrode, and Ag/AgCl (3 mol L^{-1}, KCl) electrode was used as a reference electrode.

Synthesis of $\{[Cu_{12}(pbtz)_2(Hpbtz)_2(OH)_4(H_2O)_{16}][Na(H_2O)\text{-}P_5W_{30}O_{110}]\}\cdot 16H_2O$ *(1).* $K_{12.5}Na_{1.5}[NaP_5W_{30}O_{110}]\cdot 15H_2O$ (82.4 mg, 0.01 mmol), H_2pbtz (10.7 mg, 0.05 mmol), and $CuCl_2\cdot 2H_2O$ (25.5 mg, 0.15 mmol) were mixed with 6 mL of H_2O in a cup-shaped vial. Then, the reactants were stirred for 10 min at room temperature (pH = 3.08), and the vial was capped and placed in an oven at 160 °C for 3000 min. After the reaction mixture cooled to room temperature, the resulting green block-like crystals were obtained in 40% yield (based on copper). Anal. Calcd (Found) for $C_{36}H_{92}Cu_{12}N_{28}NaO_{147}P_5W_{30}$: C, 4.45 (4.53); H, 0.95 (0.85); N, 4.03 (4.26); P, 1.59 (1.71); Na, 0.24 (0.35); Cu, 7.84 (7.72), W, 56.71 (56.43) %. IR (KBr): ν(cm^{-1}) = 3479 (s), 1619(s), 1445(m), 1162(s), 1077 (m), 1021 (w), 916 (s), 791(s), 655(s).

Synthesis of $\{[Cu_{10}(ttbz)_2(Httbz)_4(OH)_6(H_2O)_8][K(H_2O)\text{-}H_2P_5W_{30}O_{110}]\}\cdot 30H_2O$ *(2).* $K_{12.5}Na_{1.5}[NaP_5W_{30}O_{110}]\cdot 15H_2O$ (82.4 mg, 0.01 mmol), Httbz (10.7 mg, 0.05 mmol), and $CuCl_2\cdot 2H_2O$ (25.5 mg, 0.15 mmol) were mixed with 6 mL of H_2O in a cup-shaped vial. Then, the reactants were stirred for 10 min at room temperature (pH = 3.35), and the vial was capped and placed in an oven at 160 °C for 3000 min. After the reaction mixture cooled to room temperature, the resulting blue rod-like crystals were obtained in 20% yield (based on copper). Anal. Calcd (Found) for $C_{54}H_{126}Cu_{10}KN_{42}O_{155}P_5W_{30}$: C, 6.37 (6.23); H, 1.25 (1.44); N, 5.77(5.90); P, 1.52 (1.67); K, 0.38 (0.45); Cu, 6.24 (6.12); W, 54.13 (54.36) %. IR (KBr): ν(cm^{-1}) = 3447 (s), 1621(m), 1540(w), 1470(w), 1383 (w), 1163 (m), 936 (s), 796(s), 742(s).

Synthesis of $\{[Ni_6(bpz)_6(H_2O)_{16}][Na(H_2O)H_2P_5W_{30}O_{110}]\}\cdot 36H_2O$ *(3).* $K_{12.5}Na_{1.5}[NaP_5W_{30}O_{110}]\cdot 15H_2O$ (82.4 mg, 0.01 mmol), bpz (9.5 mg, 0.05 mmol), and $NiCl_2\cdot 6H_2O$ (35.7 mg, 0.15 mmol) were mixed with 6 mL of H_2O in a cup-shaped vial. Then, the reactants were stirred for 10 min at room temperature (pH = 5.16), and the vial was capped and placed in an oven at 160 °C for 3000 min. After the reaction mixture cooled to room temperature, the resulting green block-like crystals were obtained in 45% yield (based on nickel). Anal. Calcd (found) for $C_{60}H_{192}N_{24}NaNi_6O_{163}P_5W_{30}$: C, 7.28 (7.11); H, 1.95 (2.01); N, 3.39 (3.22); P, 1.56 (1.73); Na, 0.23 (0.44); Ni, 3.56 (3.68); W, 55.69 (55.78) %. IR (KBr): ν(cm^{-1}) = 3403(m), 1622(m), 1415(w), 1286(w), 1164 (s), 1078 (m), 1032(w), 912(s), 803(s), 570(s).

Synthesis of $\{[Co_4(bpz)_6(H_2O)_9][K(H_2O)H_6P_5W_{30}O_{110}]\}\cdot 46H_2O$ *(4).* $K_{12.5}Na_{1.5}[NaP_5W_{30}O_{110}]\cdot 15H_2O$ (82.4 mg, 0.01 mmol), bpz (9.5 mg, 0.05 mmol), and $Co(NO_3)_2\cdot 6H_2O$ (43.5 mg, 0.15 mmol) were mixed with 6 mL of H_2O in a cup-shaped vial. Then, the reactants were stirred for 10 min at room temperature (pH = 5.56), and the vial was capped and placed in at 160 °C for 3000 min. After the reaction mixture cooled to room temperature, the resulting red block-like crystals were obtained in 30% yield (based on cobalt). Anal. Calcd (Found) for $C_{60}H_{202}Co_4KN_{24}O_{166}P_5W_{30}$: C, 7.31 (7.45); H, 2.06 (2.15); N, 3.41 (3.60); P, 1.57 (1.33); K, 0.40 (0.62); Co, 2.39 (2.51); W, 55.93 (55.80) %. IR (KBr): ν(cm^{-1}) = 3402(s), 1628(m), 1421(w), 1283(w), 1162(s), 1069 (m), 1028(w), 940(s), 914(s), 802(s), 569(s), 533(m).

Catalytic Studies. Prior to the reaction, 48.3 mg (0.005 mmol, 1 mol % based on formula weight of **1**) of compound **1** was activated in vacuum under 40 °C for 20 min. After the material cooled to room temperature, to the Schlenk tube were added 0.5 mmol of substrates and 1 mmol of trimethylsilyl cyanide (TMSCN), then the reaction mixture was stirred at room temperature and the conversion was calculated based on ^{1}H NMR spectroscopy.

RESULTS AND DISCUSSION

Synthesis and General Characterization. Recently, many POM based hybrids have been obtained from POM−metal coordination with appropriate organic multidentate ligands to complete the assembly. However, the preparation of them consistently has been a great challenge with precipitation rather than crystals as the final products. Thus, the hydrothermal method combined with careful adjustment of pH value is a very important step to obtain the crystals in the assembly system. Although we did not deliberately adjust the pH value of the reaction system by adding acid or base, the used N-donor ligand, otherwise, plays the role of a base during the self-assembly. The crystals of **1**−**4** were collected by picking up them from abundant precipitations manually, giving the moderate yields. The measured PXRD patterns of the bulk samples of **1**−**4** match well with the simulated ones calculated from single-crystal X-ray diffractions (Figure S1 in the Supporting Information). The intensity dissimilarity between experimental and simulation PXRD patterns is due to the

DOI: 10.1021/acs.inorgchem.5b00962
Inorg. Chem. 2015, 54, 7415−7423

different orientations of the powder sample during measurements. The BVS (bond-valence sum) calculations suggest that the valences of W, Cu, Ni, and Co atoms in **1**−**4** are in the +6, +2, +2, and +2, respectively.[15] The Na ion is not presented in the central cavity of **2** and **4**, but is replaced by a K ion, which is a common phenomenon and also proved by inductively coupled plasma (ICP) spectrometer.

*Structure of {[$Cu_{12}(pbtz)_2(Hpbtz)_2(OH)_4(H_2O)_{16}$][$Na(H_2O)$-$P_5W_{30}O_{110}$]}·16$H_2O$ (**1**).* X-ray single-crystal structural analysis shows that the asymmetric unit of **1** has six crystallographically independent Cu(II) atoms, one-half of a Preyssler P_5W_{30} cluster, one $pbtz^{2-}$ and one $Hpbtz^-$ ligands, two μ_2-OH^-, eight aqua ligands, and eight lattice water molecules. The Preyssler P_5W_{30} anion acts as a dodecadentate inorganic ligand that coordinates to 12 Cu(II) ions directly (Figure 1a).

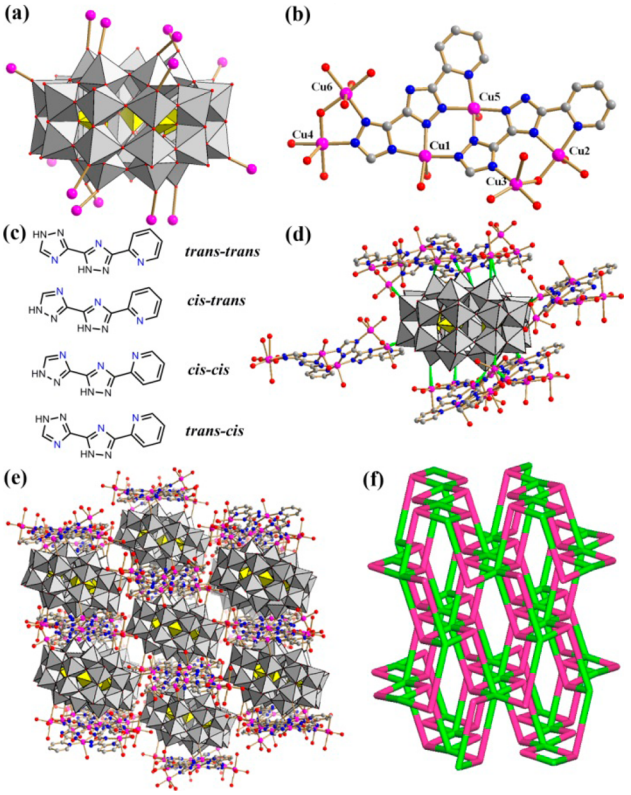

Figure 1. (a) Polyhedral representation of dodecadentate Preyssler P_5W_{30} anion in **1**. (b) Ball-and-stick showing [Cu_6(pbtz)(Hpbtz)-$(OH)_2(H_2O)_8$] subunit. (c) The possible coordination conformations of H_2pbtz ligand. (d) Six Cu_6 subunits grafted on one Preyssler P_5W_{30} anion. (e) Combined polyhedral and ball-and-stick representation of the 3D network of **1** (Cu, purple; C, gray; N, blue; O, red). (f) Representation of 3D **ant** topology of **1** (green, 6-connected P_5W_{30}; purple, 3-connected Cu_6 subunit).

Although the Preyssler P_5W_{30} anion has a high of 30 oxygen atoms on the surface available to bind to metal centers, its coordination numbers reported are not higher than 13.[12] Therefore, the dodecadentate Preyssler P_5W_{30} anion in **1** is the second highest coordination number to date. Cu1, Cu2, Cu3, Cu4, Cu5 are five-coordinated and display the distorted CuN_3O_2, CuN_2O_3, $CuNO_4$, $CuNO_4$, and CuN_4O square pyramidal geometry, respectively, whereas Cu6 is in six-coordinated $CuNO_5$ octahedral geometry (Figure 1b) (Cu−N 1.896(12)−2.044(12) Å; Cu−O 1.885(11)−-2.427(15) Å). The reactant H_2pbtz ligand shows different deprotonation forms in **1**, $pbtz^{2-}$, and $Hpbtz^-$, respectively, which coordinated to four Cu(II) ions using different N donor sites to form the [Cu_6(pbtz)(Hpbtz)$(OH)_2(H_2O)_8$] subunit. The H_2pbtz ligand has four possible coordination conformations, such as *trans*−*trans*, *cis*−*trans*, *trans*−*cis*, and *cis*−*cis* (Figure 1c). In **1**, the $pbtz^{2-}$ and $Hpbtz^-$ adopt *trans*−*trans* and *cis*−*cis* coordination conformations. In this Cu_6 subunit, Cu1 and Cu5 ions are linked by the N atoms, and the distance of Cu1···Cu5 is 4.11 Å. Cu2 and Cu3 ions are bridged by three N atoms and one μ_2-OH^- with the distance of 3.15 Å, and Cu4 and Cu6 ions are bridged by two N atoms on one triazole group and one μ_2-OH^- with the distance of 3.35 Å. In total, six [Cu_6(pbtz)(Hpbtz)-$(OH)_2(H_2O)_8$] subunits (two "above" and two "below" and the residual two "equator") are grafted on each Preyssler P_5W_{30} anion (Figure 1d), then forming the complex 3D network (Figure 1e). A better insight into the 3D framework can be done by topological analysis using TOPOS 4.0 software suite.[16] Each P_5W_{30} cluster is grafted by six Cu_6 subunits by terminal O atoms. This, thus, terms a 6-connected node. Each Cu_6 subunit is coordinated to three neighboring P_5W_{30} clusters, corresponding to a 3-connected node. As a result, the 3D network is simplified to a binodal (3,6)-connected $\{4^2{\cdot}6\}_2\{4^4{\cdot}6^2{\cdot}8^8{\cdot}10\}$ **ant** (anatase) topology (Figure 1f).

*Structure of {[$Cu_{10}(ttbz)_2(Httbz)_4(OH)_6(H_2O)_8$][$K(H_2O)$-$H_2P_5W_{30}O_{110}$]}·30$H_2O$ (**2**).* When H_2pbtz was replaced by Httbz, under the same conditions, compound **2** is obtained as a P_5W_{30} pillared-layer 3D network incorporating two-dimensional (2D) [Cu_5(ttbz)$(Httbz)_2(OH)_3(H_2O)_4$] sheets. Compound **2** crystallizes in the monoclinic $P2_1/n$ space group (Table 1), and there are one-half Preyssler P_5W_{30} cluster, five Cu(II) ions, one $ttbz^-$, two Httbz, two μ_2-OH^-, one μ_3-OH^-, and two aqua ligands in the asymmetric unit. As shown in Figure 2a, the Preyssler P_5W_{30} cluster acts as a hexapodal inorganic linker to bind six Cu(II) ions through six equatorial terminal O atoms. Cu4 and Cu5 do not directly coordinate to the P_5W_{30} cluster and are just anchored by organic ligand. Cu1, Cu3, and Cu5 ions are six-coordinate and display the distorted octahedron geometry, whereas Cu2 and Cu4 are four-coordinate square and five-coordinate square pyramidal geometries, respectively (Cu−O, 1.845(18)−2.38(2) Å; Cu−N, 1.90(2)−2.45(2) Å). The ligand also exhibits two different deprotonated forms, $ttbz^-$ and Httbz, with a ratio of 1:2. The pentadentate $ttbz^-$ uses its tetrazole and triazole groups to bridge four and one Cu(II) ions, respectively, whereas tetradebtate Httbz uses its tetrazole and triazole groups to bridge three and one Cu(II) ions, respectively. The triazole rings in one $ttbz^-$ and two Httbz are nearly coplanar with the central phenyl ring, but tetrazole rings show large dihedral angles of 69.7°, 81.9°, and 64.4°, respectively. As shown in Figure 2b, one tetrazole group, two triazole groups, two μ_2-OH^-, and one μ_3-OH^- integrate five Cu(II) to a pentanuclear unit (Cu1···Cu2 = 3.44 Å, Cu2···Cu5 = 3.39 Å, Cu3···Cu5 = 3.41 Å, Cu3···Cu4 = 3.37 Å, Cu1···Cu4 = 6.54 Å), which is progressed by bridging ligands to generate an infinite 2D sheet (Figure 2c). The Preyssler P_5W_{30} cluster acts as pillars to support the 2D sheet, giving the resultant 3D pillared network (Figure 2d).

*Structure of {[$Ni_6(bpz)_6(H_2O)_{16}$][$Na(H_2O)H_2P_5W_{30}O_{110}$]}·36$H_2O$ (**3**).* X-ray diffraction analyses show that **3** crystallizes in monoclinic $C2/c$ space group and its asymmetric unit contains one-half of Preyssler P_5W_{30} cluster, three Ni(II) ions, three bpz ligands, and eight aqua ligands. In the structure of **3**, the P_5W_{30} anion is an octadentate ligand that coordinates to

DOI: 10.1021/acs.inorgchem.5b00962
Inorg. Chem. 2015, 54, 7415−7423

Table 1. Crystal Data for 1−4[a]

	1	2	3	4
empirical formula	$C_{36}H_{26}Cu_{12}N_{28}NaO_{147}P_5W_{30}$	$C_{54}H_{46}Cu_{10}KN_{42}O_{125}P_5W_{30}$	$C_{60}H_{84}N_{24}NaNi_6O_{127}P_5W_{30}$	$C_{60}H_{84}Co_4KN_{24}O_{120}P_5W_{30}$
fw	9658.67	9628.18	9219.11	9006.67
T/K	298(2)	298(2)	298(2)	298(2)
cryst syst	monoclinic	monoclinic	monoclinic	orthorhombic
space group	$C2/c$	$P2_1/n$	$C2/c$	$Pbcn$
a/Å	29.3948(19)	21.5819(17)	25.4570(15)	27.019(2)
b/Å	21.2938(14)	19.2279(16)	21.8687(13)	38.427(3)
c/Å	28.6180(19)	25.740(2)	34.667(2)	38.738(3)
α/deg	90.00	90.00	90.00	90
β/deg	110.7220(10)	95.2863(15)	108.1429(10)	90
γ/deg	90.00	90.00	90.00	90
V/Å^3	16754.0(19)	10635.9(15)	18339.8(19)	40220(5)
Z	4	2	4	8
ρ_{calc} mg/mm^3	3.828	3.006	3.339	2.975
μ/mm^{-1}	22.158	17.270	19.475	17.549
F(000)	17 072.0	8536.0	16 408.0	31 944.0
reflns collected	41 270	52 194	45 468	160 047
indep reflns	14 711 [R(int) = 0.0379]	18 676 [R(int) = 0.0541]	16 110 [R(int) = 0.1175]	32 173 [R(int) = 0.1326]
data/restraints/params	14 711/6/1136	18 676/489/1414	16 110/39/1168	32 173/596/2196
GOF on F^2	1.027	1.054	0.889	0.923
final R indexes [$I \geq 2\sigma$ (I)]	R_1 = 0.0466, wR_2 = 0.1203	R_1 = 0.0997, wR_2 = 0.2673	R_1 = 0.0592, wR_2 = 0.1424	R_1 = 0.1146, wR_2 = 0.2506
final R indexes [all data]	R_1 = 0.0563, wR_2 = 0.1277	R_1 = 0.1197, wR_2 = 0.2796	R_1 = 0.0859, wR_2 = 0.1518	R_1 = 0.1446, wR_2 = 0.2689

[a]Data have been deposited as CCDC 1061874−1061877.

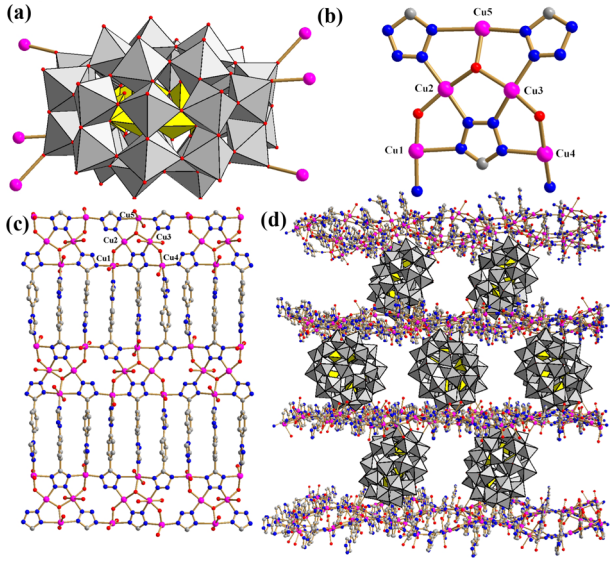

Figure 2. (a) Polyhedral representation of hexadentate Preyssler P_5W_{30} anion in **2**. (b) Ball-and-stick showing pentanuclear Cu(II) unit. (c) Ball-and-stick 2D $[Cu_{10}(ttbz)_2(Httbz)_4(OH)_6(H_2O)_8]$ sheet. (d) Combined polyhedral and ball-and-stick representation of the pillared 3D network of **2** (Cu, purple; C, gray; N, blue).

eight Ni(II) centers through two axial terminal O atoms and four equatorial terminal O atoms (Figure 3a). Each Ni atom exhibits a distorted octahedral coordination geometry (Ni−N: 2.03(18)-2.081(18) Å; Ni−O: 2.04(16)−2.131(19) Å). The coordination geometries of Ni2 and Ni3 ions are defined by two N atoms of two bpz ligands, and three aqua ligands, and one terminal O atom from the Preyssler P_5W_{30} anion. Ni1 has a diverse coordination environment, which is coordinated by two N atoms from two bpz ligands, two terminal water ligands, and two terminal O atoms from two Preyssler P_5W_{30} anions. Interestingly, bpz ligands link Ni(II) ions to give a

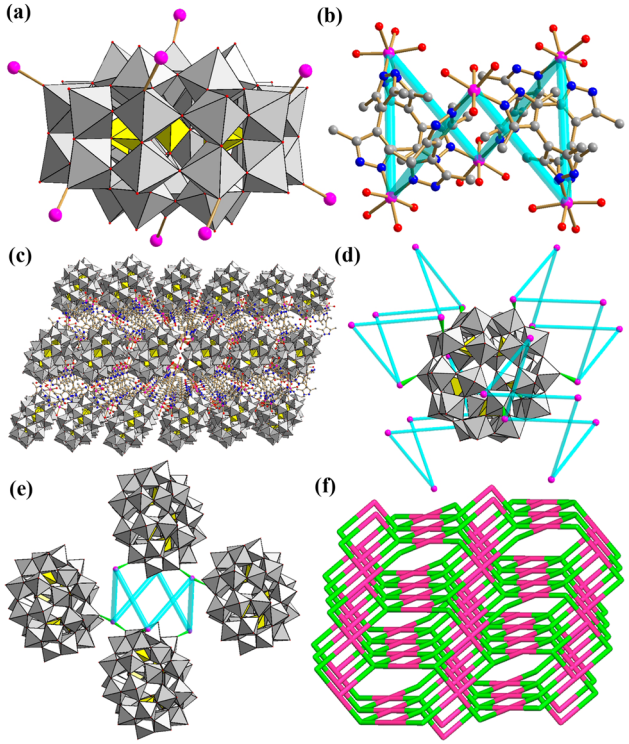

Figure 3. (a) Polyhedral representation of octadentate Preyssler P_5W_{30} anion in **3**. (b) Ball-and-stick showing $[Ni_6(bpz)_6]$ crown-like metallamacrocycle (Ni, purple; C, gray; N, blue). (c) Combined polyhedral and ball-and-stick representation of the 3D network of **3**. (d) Four $[Ni_6(bpz)_6]$ crowns grafted on one Preyssler P_5W_{30} anion. (e) Four Preyssler P_5W_{30} linked on one $[Ni_6(bpz)_6]$ crown. (f) Representation of 3D **pts** topology of **3** (purple, square 4-connected P_5W_{30}; green, tetrahedral 4-connected $[Ni_6(bpz)_6]$ crown).

DOI: 10.1021/acs.inorgchem.5b00962
Inorg. Chem. 2015, 54, 7415−7423

centrosymmetric $[Ni_6(bpz)_6]$ crown-like 42-membered metallamacrocycle (Figure 3b) with Ni(II)···Ni(II) distances of 9.47, 9.67, 9.79 Å, respectively. The Ni(II)···Ni(II)···Ni(II) angles are 65.4°, 73.6°, and 65.5°, respectively. The crowns are extended by Preyssler P_5W_{30} anions to form a complicated 3D framework (Figure 3c). Topology analysis was also performed to facilitate the understanding of such a complicated network. In the 3D network, four $[Ni_6(bpz)_6]$ crown-like metallamacrocycles are grafted on one Preyssler P_5W_{30} anion (Figure 3d), defining it as a square 4-connected node, whereas each $[Ni_6(bpz)_6]$ crown-like metallamacrocycle is bound to four Preyssler P_5W_{30} anions (Figure 3e), defining it as a tetrahedral 4-connected node; as a result, the overall 3D network topologically becomes a (4,4)-connected $\{4^2\}_2\{8^4\}$ **pts** network (Figure 3f).

Structure of $\{[Co_4(bpz)_6(H_2O)_9][K(H_2O)H_6P_5W_{30}O_{110}]\}\cdot 46H_2O$ *(**4**).* Crystallographic studies reveal that **4** crystallizes in the orthorhombic *Pbcn* space group, and there are one Preyssler P_5W_{30} cluster, four Co(II) ions, six bpz ligands, and nine aqua ligands in its asymmetric unit. In the structure of **4**, the Preyssler P_5W_{30} cluster acts as a pentadentate inorganic ligand that coordinates to five Co(II) centers directly (2 Co1, 2 Co2, 1 Co3), and the remaining one (Co4) is just coordinated to bpz and aqua ligands (Figure 4a). Co1, Co2, and Co3 are in

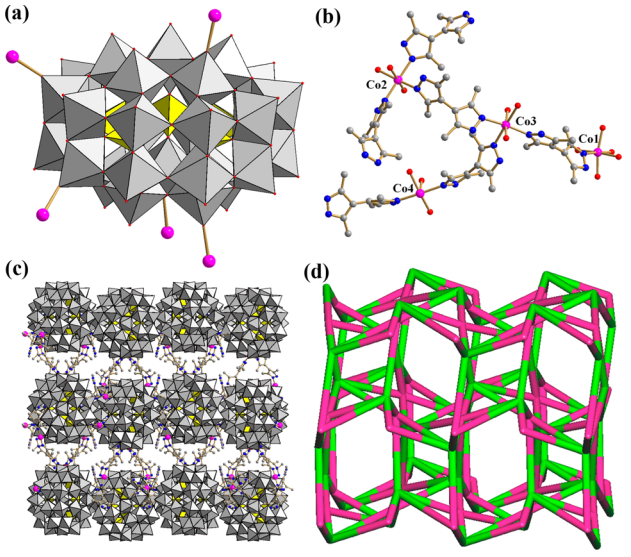

Figure 4. (a) Polyhedral representation of pentadentate Preyssler P_5W_{30} anion in **4**. (b) Ball-and-stick showing $[Co_4(bpz)_6(H_2O)_9]$ subunit (Co, purple; C, gray; N, blue). (c) Combined polyhedral and ball-and-stick representation of the 3D network of **4**. (d) Representation of 3D (5,5)-connected new topology in **4**.

the six-coordinated CoN_5O, CoN_3O_3, and CoN_3O_3 octahedron environments, whereas Co4 is five-coordinate CoN_2O_3 square pyramidal geometry (Co−N, 2.03(9)−2.15(3) Å; Co−O, 2.04(2)−2.19(3) Å). Three bpz ligands exhibit monodentate mode, and the other three exhibit bidentate bridging modes. The dihedral angles formed by twisting of two pyrazole rings in one bpz ligand are 75.2°, 68.7°, 65.7°, 72.9°, 68.7°, and 75.2°, respectively. The bidentate bridging bpz ligands extend the Co(II) centers to form a finite $[Co_4(bpz)_6(H_2O)_9]$ subunit (Figure 4b). The Preyssler P_5W_{30} clusters extend the Co_4 subunit to form the resultant 3D framework (Figure 4c). On the basis of TOPOS analysis, both the P_5W_{30} cluster and finite $[Co_4(bpz)_6(H_2O)_9]$ subunit are defined as 5-connected nodes, so the simplified network belongs to a 2-nodal (5,5)-connected topology with point symbol of $\{4^5\cdot6^4\cdot8\}\{4^5\cdot6^5\}$ (Figure 4d). The vertex symbols of the 5-connected node (P_5W_{30}) and the 5-connected node (Co_4 unit) are [4.4.4.4.4.6(2).6(3).6(4).6(4).6(4)] and [4.4.4.4.4.6(2).6(2).6(3).6(6).8(19)], respectively. To our knowledge, such a net has not been elucidated.

IR Spectra and Thermogravimetric (TG) Analysis. IR spectra of **1**−**4** were measured from 400 to 4000 cm^{-1} with KBr pellets (see Figure S2 in the Supporting Information). In IR spectra, characteristic vibration patterns of the P_5W_{30} anions, namely, ν(P−O),[17] ν(W−$O_{terminal}$), and ν(W−$O_{b/c}$),[5,10] ($O_{b/c}$: corner and edge-shared oxygen atoms) appear at 1161 and 1077, 935 and 915, and 791 and 752 cm^{-1} for **1**; 1163 and 1080, 936 and 911, and 797 and 742 cm^{-1} for **2**; 1164 and 1078, 935 and 911, and 803 and 754 cm^{-1} for **3**; and 1161 and 1069, 940 and 914, and 802 and 754 cm^{-1} for **4**, respectively. Slight splitting or shifting in characteristic peaks of P_5W_{30} might be from the coordination effect with transition-metal cations.

In order to check the thermal stabilities of **1**−**4**, thermal gravimetric (TG) analyses were carried out. As seen from Supporting Information Figure S3, the TG curves of **1**−**4** show some similarities in the 40−800 °C range. Each compound illustrates a successive weight loss step, and the observed total weight losses are 6.11%, 6.89%, 9.63%, and 8.40% for **1**−**4**, respectively, which correspond to the loss of all water molecules and N-donor ligands.

Voltammetric Behavior of ***1***- *to* ***4***-*CPEs.* As depicted in Figure 5, following the potential from −1.0 V to +1.0 V, the

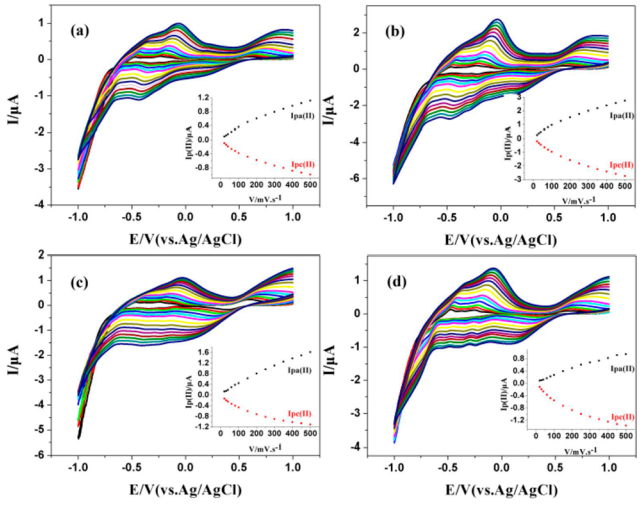

Figure 5. (a, b, c, and d) Cyclic voltammograms of the **1**-, **2**-, **3**-, and **4**-CPEs, respectively, in 1 M H_2SO_4 solution at distinct scanning rates (from inside to out: 20, 30, 40, 60, 80, 100, 120, 150, 200, 250, 300, 350, 400, 450, 500 mV s^{-1}). Inserted: The dependence of anodal and cathode peaks II current.

cyclic voltammetric behaviors of **1**, **2**, **3**, and **4** in 1 M H_2SO_4 aqueous solution at 25 °C exhibit three reduction peaks located at +0.299, −0.371, −0.650 V for **1**; +0.268, −0.377, −0.647 V for **2**; +0.241, −0.342, −0.654 V for **3**; and +0.275, −0.395, −0.637 V for **4** (vs Ag/AgCl), respectively; and three oxidation peak potentials are +0.722, −0.161, −0.412 V for **1**, +0.677, −0.144, −0.402 V for **2**, +0.756, −0.152, −0.375 V for **3**; and +0.703, −0.186, −0.431 V for **4** (on account of the CV at 100 mV s^{-1} shown in Figure S4, Supporting Information),

DOI: 10.1021/acs.inorgchem.5b00962
Inorg. Chem. 2015, 54, 7415−7423

respectively. Two pairs of redox peaks, II/II′ and III/III′, for **1**−**4** are attributed to two successive double electron processes of modified $\{P_5W_{30}\}$ polyoxoanion.[18] Redox peaks I−I′ in the positive directions for **1**−**4** should be ascribed to the redox processes of the corresponding 3d transition-metal Cu(II), Ni(II), Co(II).[19] The differences in the peak positions between parent $\{P_5W_{30}\}$ and **1**−**4** are attributed to the incorporation of the transition ions, whereas the different coordination environments around transition ions in **1**−**4** cause their different redox performance. The cathode peak potentials of compounds **1**−**4** move to the minus orientation, and the homologous anodal peak potentials move toward the plus orientation with enhancing scanning rates (Figure 5). The peak potentials vary step by step in the scanning rate range 20−500 mV s^{-1}. Moreover, the separations of peaks in the homologous anodal and cathode peaks increased; however, the mean peak potentials keep constant as a whole. The pictures of anode and cathode peak current (II) versus scanning rates (see insert pictures in Figure 5a−d) manifest that the surface-controlled redox courses of **1**- to **4**-CPEs are populated under the scanning rate of 100 mV s^{-1}, while at scanning rates over 100 mV s^{-1}, the peak electricity was proportional to the square root of the scanning rate, indicating that redox courses are diffusion-controlled.[20] It is also noteworthy that **1**- to **4**-CPEs possess the high stability. When the potential scope is held in −1.0 and 1.0 V, the peak electricity remains nearly constant higher than 300 cycles at a scanning rate of 100 mV s^{-1}.

*Electrocatalytic Activity of **1**- to **4**-CPEs for the Reduction of H_2O_2.* Figure 6 reveals cyclic voltammograms for the

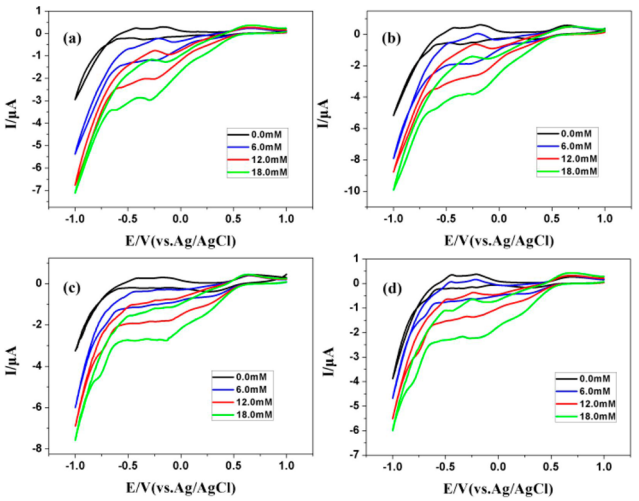

Figure 6. (a, b, c, and d) Cyclic voltammograms of the **1**-, **2**-, **3**-, and **4**-CPES, respectively, in 1 M H_2SO_4 solution containing 0.0, 6.0, 12.0, 18.0 mM H_2O_2. scan rates: 40 mV s^{-1}.

electrocatalytic reduction of H_2O_2 at **1**-, **2**-, **3**- and **4**-CPEs in 1 M H_2SO_4 aqueous solution with the potential changing from −1.0 to 1.0 V. With enhancing H_2O_2 concentration (from 0.0 to 18.0 mM), the peak currents of II and III increased step by step while the corresponding oxidation peak currents remarkably reduced, suggesting that H_2O_2 is mediated by the W of $P_5W_{30}O_{110}^{14-}$ polyanions.[20] It is worth pointing out that there is no decrease in the associated anodic peak current for a 3d transition metal with successive additions of H_2O_2, indicating they are redox silent for H_2O_2. In contrast, the reduction of H_2O_2 at a bare electrode normally needs a large overpotential, and no apparent behavior happened at a bare CPE. The results show that **1**- to **4**-CPEs have moderate electric catalytic ability for the reduction of H_2O_2.

Catalytic Activity. As we know, cyanosilylation reaction for cyanalcohol is widely used to test the Lewis acid catalysis of coordination polymers.[21] Compound **1** was measured as an acid catalyst for the cyanosilylation of carbonyl compounds. Before the catalytic test, compound **1** was activated at 40 °C under vacuum for 20 min. The cyanosilylation was carried out in the presence of **1** with a 1:2 molar ratio of the selected carbonyls and trimethylsilyl cyanide (TMSCN) for 24 h at room temperature under nitrogen through a heterogeneous manner. The conversions were calculated on the basis of ^1H NMR spectroscopy (see Supporting Information). The results in Table 2 showed that the 1 mol % loading of catalyst **1** (0.005 mmol) caused moderate catalytic activity with about 61.7% conversion for benzaldehyde. The employment of such a catalyst could be expanded to other carbonyl derivatives with different catalysis performance, which may be explained by steric hindrance and electron effects. For ketones, the very low catalytic activity is due to the low reactivity of ketones compared with aldehydes. The size selectivity of the substrate suggested that cyanosilylation indeed occurs in the channels of the POM instead of the external surfaces.[22]

Table 2. Results for the Catalytic Cyanosilylation of Aldehydes in the Presence of 1.

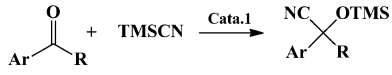

Entry	Aldehyde/Ketone	Conversion (%)
1	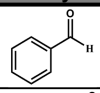	61.7
2	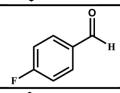	36.8
3	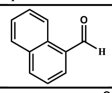	40.6
4	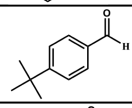	10.8
5	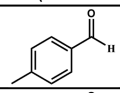	10.1
6	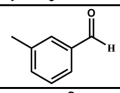	8.5
7	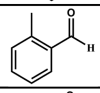	69.0
8		~0
9	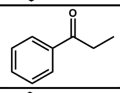	~0
10	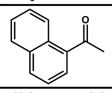	~0

Reaction conditions: aldehyde/ketone, 0.5mmol; TMSCN, 1mmol; catalyst **1**, 0.005mmol (1%); at room temperature under N_2 for 24h.

DOI: 10.1021/acs.inorgchem.5b00962
Inorg. Chem. 2015, 54, 7415−7423

Although the possible mechanistic pathway cannot be definitely established, the catalytic reaction should involve an intermediate species with the substrate coordinated to the unsaturated Cu(II) atoms produced in the activation process. The octahedral environment of Cu(II) should not be an impediment for copper-containing species to be involved in the catalytic cycle, because its coordination environment can vary, especially when one or some water molecules are terminal ligands, which could be pulled off by activation, and then make Cu(II) an active site for Lewis acid catalysis.

Magnetic Properties. The dc magnetic susceptibility was measured on polycrystalline samples in the 2−300 K temperature range in an applied magnetic field of 1 kOe for **1** and **2**. The data was corrected for three temperature independent contributions: sample holder, diamagnetism of core electrons as obtained from Pascal's tables, and temperature independent paramagnetsim.[23] The temperature dependent susceptibility per mole χ_M of the **1** and its effective magnetic moment p_{eff} calculated per Cu atom are shown on Figure 7a.

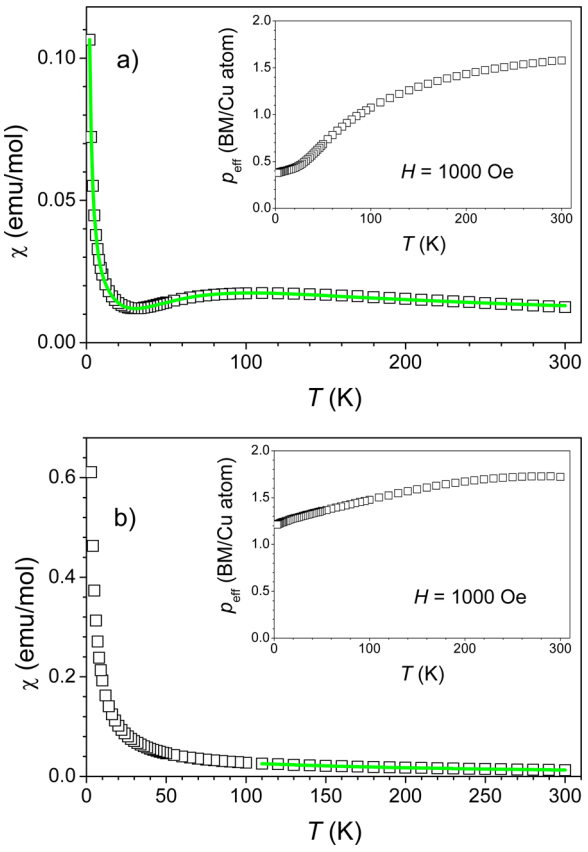

Figure 7. Temperature dependent susceptibility and magnetic moment (insets) of **1** (a) and **2** (b). Full lines are fits with eq 1 for **1** and Curie−Weiss model for **2**.

The susceptibility shows a local maximum at approximately 110 K indicating an antiferromagnetic interaction between copper magnetic moments. Below 20 K the susceptibility increases approximately inversely with decreasing temperature exhibiting so-called Curie tail. The effective magnetic moment calculated per Cu atom is 1.58 μ_B at room temperature. This value is reduced from the expected value for noninteracting Cu^{2+} ion with spin $S = {}^1/_2$ (p_{eff} = 1.9 μ_B) and decreases with decreasing temperature.[24] Below 20 K the effective magnetic moment p_{eff} obtains an almost constant value of p_{eff} = 0.4 μ_B. From the measured temperature dependent χ_M and p_{eff} we can conclude the antiferromagnetic interaction between Cu^{2+} ions is effective already at room temperature. In consideration of the structure of **1**, three unique dimeric units with different bridges can be observed in an asymmetric unit of **1**: Cu1—Cu5 dimer with two —N═N— bridges; Cu4−Cu6 with two different bridges, —N═N— and μ_2-OH^-; and Cu2—Cu3 with a single μ_2-OH^- bridge. Browsing the literature we have found the —N═N— and μ_2-OH^- bridges can produce very different strengths of antiferromagnetic interaction, for example, a relatively strong interaction J = −177 K for Cu—N—N—Cu bridge (angle 150.6°) and a weak exchange J = −66 K for Cu—O—Cu (angle 141.7°) was found in copper(II) complexes of alkoxy diazine ligands.[25] On the other hand much stronger exchange J = −467 K for Cu—O—Cu (angle 180°) was determined in dinuclear Cu(II) metallacycle with single Cu—O—Cu bridges.[26] As in **1**, the Cu—O—Cu angle (125°) is far from 180°; we expect a relatively weak exchange through the Cu—O—Cu bridge. The interaction Hamiltonian was written in the form $H_{int} = -2J_1\boldsymbol{S}_1\cdot\boldsymbol{S}_5 - 2J_2\boldsymbol{S}_4\cdot\boldsymbol{S}_6 - 2J_3\boldsymbol{S}_2\cdot\boldsymbol{S}_3$ with three exchange interactions J_1, J_2, and J_3 and spins $\boldsymbol{S}_i = {}^1/_2$ that corresponds to Cu(i) ions. We obtained the modified Bleaney−Bowers equation[23] as the following:

$$\chi = 2\left((1-\rho)\left[\frac{2N_A g^2\mu_B^2}{k_B T(3+e^{-2J_1/k_B T})} + \frac{2N_A g^2\mu_B^2}{k_B T(3+e^{-2J_2/k_B T})} + \frac{2N_A g^2\mu_B^2}{k_B T(3+e^{-2J_3/k_B T})}\right] + \rho\frac{N_A g^2\mu_B^2}{2k_B T}\right) \quad (1)$$

Here, the factor of 2 accounts for two of each of three dimeric units per chemical formula. The last term in eq 1 accounts for noninteracting paramagnetic species with the factor ρ as a molar fraction of these paramagnetic moments, N_A is the Avogadro number, μ_B the Bohr magneton, and k_B the Boltzmann constant. The best fit to the experimental data was obtained (full green line in Figure 7a) with J_1/k_B = −410 K, J_2/k_B = −124 K, J_1/k_B = −71 K, and ρ = 12%, while g = 2.1 constrained. We have to stress that the fitting of the susceptibility with eq 1 cannot give us the information regarding the exchange interaction J_1, J_2, and J_3 corresponding to a particular bridge. According to the above discussion we tentatively ascribe the strongest exchange interaction to the two —N═N— bridges and the weakest one to the single μ_2-OH^- bridge.

A temperature dependent susceptibility of **2** (Figure 7b) shows continuous increase on decreasing temperature from 300 K down to 2 K. The Curie−Weiss fit $\chi = C/(T-\vartheta)$ is applied for T > 100 K as shown as a full line in Figure 7b. The obtained Curie constant C and calculated effective magnetic moment per Cu atom of p_{eff} = 1.8 μ_B confirm a divalent oxidation state of Cu ions. However, a negative Curie−Weiss temperature ϑ = −107 K and decrease of the effective magnetic moment with decreasing temperature indicate an appreciable antiferromagnetic exchange interaction between Cu magnetic moments. The antiferromagnetic interaction is secured by the Cu−O−Cu bridges as we have found already for **1**. According to a relatively large negative Curie−Weiss temperature, one should expect a maximum in the measured χ_T and decrease of the susceptibility below 100 K as for **2**. The absence of these features can be contributed to the specific geometric arrangements of the magnetic moment. Copper atoms in **2** are collected in the

DOI: 10.1021/acs.inorgchem.5b00962
Inorg. Chem. 2015, 54, 7415−7423

isolated groups of five atoms with the simplified geometry shown in Figure 2b. With the assumption of AFM exchange interaction between nearest neighbor Cu(II) magnetic moments, it is clear that this configuration leads to a highly frustrated system as no configuration of magnetic moments can simultaneously minimize energy of all the bonds.

CONCLUSIONS

In conclusion, four P_5W_{30} based inorganic−organic hybrid materials were synthesized hydrothermally. The synthesis of these compounds with success demonstrates that the Preyssler P_5W_{30} polyanions could link with first-row transition-metal ions (e.g., Cu(II), Ni(II), or Co(II) ions) in the presence of different N-donor polydentate ligands. In **1**−**4**, Preyssler-type P_5W_{30} anions exhibit dodeca-, hexa-, octa-, and pentadentate modes, respectively, to support the transition-metal compounds subunits. The obtained **1**−**4** exhibit different 3D networks ranging from (3,6)-connected **ant**, pillared-layer 3D network, (4,4)-connected **pts**, and (5,5)-connected $\{4^5{\cdot}6^4{\cdot}8\}\{4^5{\cdot}6^5\}$ networks, respectively. The properties about electrochemistry of compounds **1**−**4** have been studied, and they show electrocatalytic abilities on the reduction of hydrogen peroxide. Magnetic susceptibility tests demonstrate antiferromagnetism coupling within hexa- and pentanuclear Cu(II) units in **1** and **2**. Furthermore, the catalytic activities of **1** in the cyanosilylation of aldehydes have been investigated.

ASSOCIATED CONTENT

Supporting Information

Tables, crystal data in CIF files, IR, CV, TGA, powder X-ray diffractogram for **1**−**4**, and ^{1}H NMR spectra for catalysis tests of **1**. The Supporting Information is available free of charge on the ACS Publications website at DOI: 10.1021/acs.inorgchem.5b00962.

AUTHOR INFORMATION

Corresponding Author

*E-mail: dsun@sdu.edu.cn.

Author Contributions

T.-P.H. and Y.-Q.Z. contributed equally.

Notes

The authors declare no competing financial interest.

ACKNOWLEDGMENTS

This work was supported by the NSFC (Grant No. 21201110), Research Award Fund for Outstanding Middle-Aged and Young Scientist of Shandong Province (BS2013CL010), the International Scientific and Technological Cooperation Projects of Shanxi Province (No: 2015081043), "131" Leading Talents Project in Colleges and Universities, Science and Technology Innovation Project of Shanxi Province (No: 2014101002).

REFERENCES

(1) (a) Pope, M. T. *Heteropoly and Isopoly Oxometalates*; Springer: Berlin, 1983. (b) Hill, C. L. *Chem. Rev.* **1998**, *98*, 1−2. (c) Hagrman, P. J.; Hagrman, D.; Zubieta, J. *Angew. Chem., Int. Ed.* **1999**, *38*, 2638−2684. (d) Müller, A.; Serain, C. *Acc. Chem. Res.* **2000**, *33*, 2−10. (e) Long, D. L.; Burkholder, E.; Cronin, L. *Chem. Soc. Rev.* **2007**, *36*, 105−121. (f) Niu, J. Y.; Zhang, X. Q.; Yang, D. H.; Zhao, J. W.; Ma, P. T.; Kortz, U.; Wang, J. P. *Chem. - Eur. J.* **2012**, *18*, 6759−6762.

(2) (a) Khan, M. I.; Yohannes, E.; Doedens, R. J. *Angew. Chem., Int. Ed.* **1999**, *38*, 1292−1294. (b) Fukaya, K.; Yamase, T. *Angew. Chem., Int. Ed.* **2003**, *42*, 654−658. (c) Wu, C. D.; Lu, C. Z.; Zhuang, H. H.; Huang, J. S. *J. Am. Chem. Soc.* **2002**, *124*, 3836−3837. (d) Wang, X. L.; Qin, C.; Wang, E. B.; Su, Z. M.; Li, Y. G.; Xu, L. *Angew. Chem., Int. Ed.* **2006**, *45*, 7411−7414. (e) Wang, X. L.; Bi, Y. F.; Chen, B. K.; Lin, H. Y.; Liu, G. C. *Inorg. Chem.* **2008**, *47*, 2442−2448. (f) Han, Q. X.; He, C.; Zhao, M.; Qi, B.; Niu, J. Y.; Duan, C. Y. *J. Am. Chem. Soc.* **2013**, *135*, 10186−10189. (g) Zhang, S. R.; Du, D. Y.; Tan, K.; Qin, J. S.; Dong, H. Q.; Li, S. L.; He, W. W.; Lan, Y. Q.; Shen, P.; Su, Z. M. *Chem. - Eur. J.* **2013**, *19*, 11279−11286.

(3) (a) Müller, A.; Shah, S. Q. N.; Bögge, H.; Schmidtmann, M. *Nature* **1999**, *397*, 48−50. (b) Xu, L.; Lu, M.; Xu, B. B.; Wei, Y. G.; Peng, Z. H.; Powell, D. R. *Angew. Chem., Int. Ed.* **2002**, *41*, 4129−4132. (c) Kögerler, P.; Cronin, L. *Angew. Chem., Int. Ed.* **2005**, *44*, 844−846. (d) Zhang, J.; Song, Y. F.; Cronin, L.; Liu, T. B. *J. Am. Chem. Soc.* **2008**, *130*, 14408−14409. (e) Yin, Q. S.; Tan, J. M.; Besson, C.; Geletii, Y. V.; Musaev, D. G.; Kuznetsov, A. E.; Luo, Z.; Hardcastle, K. I.; Hill, C. L. *Science* **2010**, *328*, 342−345. (f) Sun, C. Y.; Liu, S. X.; Liang, D. D.; Shao, K. Z.; Ren, Y. H.; Su, Z. M. *J. Am. Chem. Soc.* **2009**, *131*, 1883−1888. (g) Wu, H.; Yang, J.; Su, Z. M.; Batten, S. R.; Ma, J. F. *J. Am. Chem. Soc.* **2011**, *133*, 11406−11409.

(4) (a) Chen, L.; Jiang, F. L.; Lin, Z. Z.; Zhou, Y. F.; Yue, C. Y.; Hong, M. C. *J. Am. Chem. Soc.* **2005**, *127*, 8588−8589. (b) Wu, C. D.; Lu, C. Z.; Zhuang, H. H.; Huang, J. S. *J. Am. Chem. Soc.* **2002**, *124*, 3836−3837. (c) Zheng, S. L.; Yang, J. H.; Yu, X. L.; Chen, X. M.; Wong, W. T. *Inorg. Chem.* **2004**, *43*, 830−838. (d) Zhang, L. R.; Shi, Z.; Yang, G. Y.; Chen, X. M.; Feng, S. H. *J. Chem. Soc., Dalton. Trans.* **2000**, 275−278. (e) Zheng, S. T.; Zhang, J.; Yang, G. Y. *Inorg. Chem.* **2005**, *44*, 2426−2430. (f) Bu, X. H.; Chen, W.; Du, M.; Biradha, K.; Wang, W. Z.; Zhang, R. H. *Inorg. Chem.* **2002**, *41*, 437−439.

(5) (a) Wang, X. L.; Li, J.; Tian, A. X.; Lin, H. Y.; Liu, G. C.; Hu, H. L. *Inorg. Chem. Commun.* **2011**, *14*, 103−106. (b) Yvon, C.; Macdonell, A.; Buchwald, S.; Surman, A. J.; Follet, N.; Alex, J.; Long, D. L.; Cronin, L. *Chem. Sci.* **2013**, *4*, 3810−3817. (c) Wu, P. F.; Yin, P. C.; Zhang, J.; Hao, J.; Xiao, Z. C.; Wei, Y. G. *Chem. - Eur. J.* **2011**, *17*, 12002−12005. (d) Kikukawa, Y.; Yamaguchi, K.; Mizuno, N. *Angew. Chem., Int. Ed.* **2010**, *49*, 6096−6100. (e) Son, J. H.; Ohlin, C. A.; Johnson, R. L.; Yu, P.; Casey, W. H. *Chem. - Eur. J.* **2013**, *19*, 5191−5197. (f) Sugahara, K.; Kimura, T.; Kamata, K.; Yamaguchi, K.; Mizuno, N. *Chem. Commun.* **2012**, *48*, 8422−8424. (g) Wang, L. S.; Yin, P. C.; Zhang, J.; Hao, J.; Lv, C. L.; Xiao, F. P.; Wei, Y. G. *Chem. - Eur. J.* **2011**, *17*, 4796−4801.

(6) (a) Chiang, M. H.; Antonio, M. R.; Williams, C. W.; Soderholm, L. *Dalton. Trans.* **2004**, 801−806. (b) Soderholm, L.; Antonio, M. R.; Skanthakumar, S.; Williams, C. W. *J. Am. Chem. Soc.* **2002**, *124*, 7290−7291. (c) Huang, M.; Bi, L.; Shen, Y.; Liu, B.; Dong, S. *J. Phys. Chem. B* **2004**, *108*, 9780−9786. (d) Harrup, M. K.; Hill, C. L. *Inorg. Chem.* **1994**, *33*, 5448−5455.

(7) Zhang, Z. M.; Yao, S.; Qi, Y. F.; Li, Y. G.; Wang, Y. H.; Wang, E. B. *Dalton. Trans.* **2008**, 3051−3053.

(8) (a) Cardona-Serra, S.; Clemente-Juan, J. M.; Coronado, E.; Gaita-Ariño, A.; Camón, A.; Evangelisti, M.; Luis, F.; Martínez-Pérez, M. J.; Sese, J. *J. Am. Chem. Soc.* **2012**, *134*, 14982−14990. (b) Lehmann, J.; Gaita-Arino, A.; Coronado, E.; Loss, D. *Nat. Nanotechnol.* **2007**, *2*, 312−317. (c) Martínez-Pérez, M. J.; Montero, O.; Evangelisti, M.; Luis, F.; Sesé, J.; Cardona-Serra, S.; Coronado, E. *Adv. Mater.* **2012**, *24*, 4301−4305.

(9) (a) Hussain, F.; Kortz, U.; Keita, B.; Nadjo, L.; Pope, M. T. *Inorg. Chem.* **2006**, *45*, 761−766. (b) Dickman, M. H.; Gama, G. J.; Kim, K. C.; Pope, M. T. *J. Cluster Sci.* **1996**, *7*, 567−583.

(10) Lu, Y.; Li, Y. G.; Wang, E. B.; Xu, X. X.; Ma, Y. *Inorg. Chim. Acta* **2007**, *360*, 2063−2070.

(11) Qin, C.; Song, X. Z.; Su, S. Q.; Dang, S.; Feng, J.; Song, S. Y.; Hao, Z. M.; Zhang, H. J. *Dalton. Trans.* **2012**, *41*, 2399−2407.

(12) Li, Y. Y.; Zhao, J. W.; Wei, Q.; Yang, B. F.; He, H.; Yang, G. Y. *Chem. - Asian J.* **2014**, *9*, 858−867.

(13) Zhao, Y. Q.; Yu, K.; Wang, L. W.; Wang, Y.; Wang, X. P.; Sun, D. *Inorg. Chem.* **2014**, *53*, 11046−11050.

(14) Ginsberg, A. P. *Inorganic Syntheses*; Wiley: New York, 1990; Vol. 27, p 105.

DOI: 10.1021/acs.inorgchem.5b00962
Inorg. Chem. 2015, 54, 7415−7423

(15) Brown, I. D.; Altermatt, D. *Acta Crystallogr., Sect. B: Struct. Sci.* **1985**, *41*, 244−247.
(16) (a) Carlucci, L.; Ciani, G.; Proserpio, D. M.; Mitina, T. G.; Blatov, V. A. *Chem. Rev.* **2014**, *114*, 7557−7580. (b) Blatov, V. A. *Struct. Chem.* **2012**, *23*, 955. (c) Blatov, V. A.; Shevchenko, A. P.; Proserpio, D. M. *Cryst. Growth Des.* **2014**, *14*, 3576−3586.
(17) Alizadeh, M. H.; Harmalker, S. P.; Jeannin, Y.; Frere, J. M.; Pope, M. T. *J. Am. Chem. Soc.* **1985**, *107*, 2662−2669.
(18) (a) Yang, C. Y.; Zhang, L. C.; Wang, Z. J.; Wang, L.; Li, X. H.; Zhu, Z. M. *J. Solid State Chem.* **2012**, *194*, 270−276. (b) Zhang, Z. M.; Yao, S.; Qi, Y. F.; Li, Y. G.; Wang, Y. H.; Wang, E. B. *Dalton. Trans.* **2008**, 3051−3053. (c) Hussain, F.; Kortz, U.; Keita, B.; Nadjo, L.; Pope, M. T. *Inorg. Chem.* **2006**, *45*, 761−766. (d) Wang, X. L.; Li, J.; Tian, A. X.; Lin, H. Y.; Liu, G. C.; Hu, H. L. *Inorg. Chem. Commun.* **2011**, *14*, 103−106. (e) Antonio, M. R.; Chiang, M. H. *Inorg. Chem.* **2008**, *47*, 8278−8285.
(19) (a) Zhang, Z. M.; Yao, S.; Qi, Y. F.; Li, Y. G.; Wang, Y. H.; Wang, E. B. *Dalton. Trans.* **2008**, 3051−3053. (b) Antonio, M. R.; Chiang, M. H. *Inorg. Chem.* **2008**, *47*, 8278−8285.
(20) Martel, D.; Kuhn, A. *Electrochim. Acta* **2000**, *45*, 1829−1836.
(21) Kajiwara, T.; Higuchi, M.; Yuasa, A.; Higashimura, H.; Kitagawa, S. *Chem. Commun.* **2013**, *49*, 10459−10461.
(22) Lee, J.; Farha, O. K.; Roberts, J.; Scheidt, K. A.; Nguyen, S. T.; Hupp, J. T. *Chem. Soc. Rev.* **2009**, *38*, 1450−1459.
(23) Kahn, O. *Molecular Magnetism*; VCH Publishing: Weinheim, Germany, 1993.
(24) Ashcroft, N. W.; Mermin, N. D. *Solid State Physics*; Saunders College Publishing: Philadelphia, PA, 1976.
(25) Grove, H.; Kelly, T. L.; Thompson, L. K.; Zhao, L.; Xu, Z.; Abedin, T. S. M.; Miller, D. O.; Goeta, A. E.; Wilson, C.; Howard, J. A. K. *Inorg. Chem.* **2004**, *43*, 4278−4288.
(26) Reger, D. L.; Pascui, A. E.; Foley, E. A.; Smith, M. D.; Jezierska, J.; Ozarowski, A. *Inorg. Chem.* **2014**, *53*, 1975−1988.

DOI: 10.1021/acs.inorgchem.5b00962
Inorg. Chem. 2015, 54, 7415−7423